The Astrophysical Journal, 756:48 (9pp), 2012 September 1 doi:10.1088/0004-637X/756/1/48

A NEW TYPE OF AMBIGUITY IN THE PLANET AND BINARY INTERPRETATIONS OF CENTRAL PERTURBATIONS OF HIGH-MAGNIFICATION GRAVITATIONAL MICROLENSING EVENTS

J.-Y. Choi[1], I.-G. Shin[1], C. Han[1,62,64], A. Udalski[2,61], T. Sumi[3,63], A. Gould[4,64], V. Bozza[5,6,65], M. Dominik[7,65,66], P. Fouqué[8,67], K. Horne[7,68],

and

M. K. Szymański[2], M. Kubiak[2], I. Soszyński[2], G. Pietrzyński[2,9], R. Poleski[2], K. Ulaczyk[2], P. Pietrukowicz[2], S. Kozłowski[2], J. Skowron[4], Ł. Wyrzykowski[2,10]

(The OGLE Collaboration)

F. Abe[11], D. P. Bennett[12], I. A. Bond[13], C. S. Botzler[14], P. Chote[15], M. Freeman[14], A. Fukui[16], K. Furusawa[11], Y. Itow[11], S. Kobara[11], C. H. Ling[13], K. Masuda[11], Y. Matsubara[11], N. Miyake[11], Y. Muraki[11], K. Ohmori[11], K. Ohnishi[17], N. J. Rattenbury[14], To. Saito[18], D. J. Sullivan[15], D. Suzuki[3], K. Suzuki[11], W. L. Sweatman[13], S. Takino[11], P. J. Tristram[15], K. Wada[3], P. C. M. Yock[14]

(The MOA Collaboration)

D. M. Bramich[19], C. Snodgrass[20], I. A. Steele[21], R. A. Street[22], Y. Tsapras[22,23]

(The RoboNet Collaboration)

K. A. Alsubai[24], P. Browne[7], M. J. Burgdorf[25,26], S. Calchi Novati[5,27], P. Dodds[7], S. Dreizler[28], X.-S. Fang[29], F. Grundahl[30], C.-H. Gu[29], S. Hardis[31], K. Harpsøe[31,32], T. C. Hinse[31,33,34], A. Hornstrup[35], M. Hundertmark[7,28], J. Jessen-Hansen[30], U. G. Jørgensen[31,32], N. Kains[36], E. Kerins[37], C. Liebig[7], M. Lund[30], M. Lunkkvist[30], L. Mancini[38,39], M. Mathiasen[31], M. T. Penny[37,4], S. Rahvar[40,41], D. Ricci[42], G. Scarpetta[5,27,6], J. Skottfelt[31], J. Southworth[43], J. Surdej[42], J. Tregloan-Reed[43], J. Wambsganss[44], O. Wertz[42]

(The MiNDSTEp Consortium)

L. A. Almeida[45], V. Batista[4], G. Christie[46], D. L. DePoy[47], Subo Dong[48], B. S. Gaudi[4], C. Henderson[4], F. Jablonski[45], C.-U. Lee[34], J. McCormick[49], D. McGregor[4], D. Moorhouse[50], T. Natusch[46,51], H. Ngan[46], R. W. Pogge[4], T.-G. Tan[52], G. Thornley[50], J. C. Yee[4]

(The μFUN Collaboration)

M. D. Albrow[53], E. Bachelet[8], J.-P. Beaulieu[54], S. Brillant[55], A. Cassan[54], A. A. Cole[56], E. Corrales[54], C. Coutures[54], S. Dieters[56], D. Dominis Prester[57], J. Donatowicz[58], J. Greenhill[56], D. Kubas[55,54], J.-B. Marquette[54], J. W. Menzies[59], K. C. Sahu[60], and M. Zub[44]

(The PLANET Collaboration)

[1] Department of Physics, Institute for Astrophysics, Chungbuk National University, Cheongju 371-763, Republic of Korea
[2] Warsaw University Observatory, Al. Ujazdowskie 4, 00-478 Warszawa, Poland
[3] Department of Earth and Space Science, Osaka University, Osaka 560-0043, Japan
[4] Department of Astronomy, Ohio State University, 140 West 18th Avenue, Columbus, OH 43210, USA
[5] Dipartimento di Fisica "E. R. Caianiello," Università degli Studi di Salerno, Via Ponte Don Melillo, I-84084 Fisciano (SA), Italy
[6] INFN, Gruppo Collegato di Salerno, Sezione di Napoli, Via S. Allende, I-84081 Baronissi (Salerno), Italy
[7] SUPA, University of St Andrews, School of Physics & Astronomy, North Haugh, St Andrews KY16 9SS, UK
[8] IRAP, Université de Toulouse, CNRS, 14 Avenue Edouard Belin, F-31400 Toulouse, France
[9] Departamento de Astronomia, Universidad de Concepción, Casilla 160-C, Concepción, Chile
[10] Institute of Astronomy, University of Cambridge, Madingley Road, Cambridge CB3 0HA, UK
[11] Solar-Terrestrial Environment Laboratory, Nagoya University, Nagoya 464-8601, Japan
[12] Department of Physics, University of Notre Dame, 225 Nieuwland Science Hall, Notre Dame, IN 46556-5670, USA
[13] Institute of Information and Mathematical Sciences, Massey University, Private Bag 102-904, North Shore Mail Centre, Auckland, New Zealand
[14] Department of Physics, University of Auckland, Private Bag 92-019, Auckland 1001, New Zealand
[15] School of Chemical and Physical Sciences, Victoria University of Wellington, P.O. Box 60, Wellington, New Zealand
[16] Okayama Astrophysical Observatory, NAOJ, Okayama 719-0232, Japan
[17] Nagano National College of Technology, Nagano 381-8550, Japan
[18] Tokyo Metropolitan College of Aeronautics, Tokyo 116-8523, Japan
[19] European Southern Observatory, Karl-Schwarzschild-Str. 2, D-85748 Garching bei München, Germany
[20] Max Planck Institute for Solar System Research, Max-Planck-Str. 2, D-37191 Katlenburg-Lindau, Germany
[21] Astrophysics Research Institute, Liverpool John Moores University, Liverpool CH41 1LD, UK
[22] Las Cumbres Observatory Global Telescope Network, 6740B Cortona Drive, Goleta, CA 93117, USA
[23] School of Physics and Astronomy, Queen Mary University of London, Mile End Road, London E1 4NS, UK
[24] Qatar Foundation, P.O. Box 5825, Doha, Qatar
[25] Deutsches SOFIA Institut, Universität Stuttgart, Pfaffenwaldring 31, D-70569 Stuttgart, Germany
[26] SOFIA Science Center, NASA Ames Research Center, Mail Stop N211-3, Moffett Field CA 94035, USA
[27] Istituto Internazionale per gli Alti Studi Scientifici (IIASS), I-84019 Vietri Sul Mare (SA), Italy
[28] Institut für Astrophysik, Georg-August-Universität, Friedrich-Hund-Platz 1, D-37077 Göttingen, Germany
[29] National Astronomical Observatories/Yunnan Observatory, Joint laboratory for Optical Astronomy, Chinese Academy of Sciences, Kunming 650011, China
[30] Department of Physics and Astronomy, Aarhus University, Ny Munkegade 120, DK-8000 Århus C, Denmark
[31] Niels Bohr Institute, University of Copenhagen, Juliane Maries vej 30, DK-2100 Copenhagen, Denmark
[32] Centre for Star and Planet Formation, Geological Museum, Øster Voldgade 5, DK-1350 Copenhagen, Denmark
[33] Armagh Observatory, College Hill, Armagh BT61 9DG, UK
[34] Korea Astronomy and Space Science Institute, 776 Daedukdae-ro, Yuseong-gu, Daejeon 305-348, Republic of Korea
[35] Danmarks Tekniske Universitet, Institut for Rumforskning og-teknologi, Juliane Maries Vej 30, DK-2100 København, Denmark

[36] ESO Headquarters, Karl-Schwarzschild-Str. 2, D-85748 Garching bei München, Germany
[37] Jodrell Bank Centre for Astrophysics, University of Manchester, Oxford Road, Manchester M13 9PL, UK
[38] Max Planck Institute for Astronomy, KÄonigstuhl 17, D-69117 Heidelberg, Germany
[39] International Institute for Advanced Scientific Studies, I-84019 Vietri Sul Mare (SA), Italy
[40] Department of Physics, Sharif University of Technology, P.O. Box 11155-9161, Tehran, Iran
[41] Perimeter Institue for Theoretical Physics, 31 Caroline Street North, Waterloo, ON N2L2Y5, Canada
[42] Institut d'Astrophysique et de Géophysique, Allée du 6 Août 17, Sart Tilman, Bât. B5c, B-4000 Liège, Belgium
[43] Astrophysics Group, Keele University, Staffordshire ST5 5BG, UK
[44] Astronomisches Rechen-Institut, Zentrum für Astronomie der Universität Heidelberg (ZAH), Mönchhofstr. 12-14, D-69120 Heidelberg, Germany
[45] Instituto Nacional de Pesquisas Espaciais, São José dos Campos, SP, Brazil
[46] Auckland Observatory, Auckland, New Zealand
[47] Department of Physics, Texas A&M University, College Station, TX 77843, USA
[48] Institute for Advanced Study, Einstein Drive, Princeton, NJ 08540, USA
[49] Farm Cove Observatory, Centre for Backyard Astrophysics, Pakuranga, Auckland, New Zealand
[50] Kumeu Observatory, Kumeu, New Zealand
[51] Institute for Radiophysics and Space Research, AUT University, Auckland, New Zealand
[52] Perth Exoplanet Survey Telescope, Perth, Australia
[53] Department of Physics and Astronomy, University of Canterbury, Private Bag 4800, Christchurch 8020, New Zealand
[54] UPMC-CNRS, UMR 7095, Institut d'Astrophysique de Paris, 98bis Boulevard Arago, F-75014 Paris, France
[55] European Southern Observatory, Casilla 19001, Vitacura 19, Santiago, Chile
[56] School of Mathematics and Physics, University of Tasmania, Private Bag 37, Hobart, TAS 7001, Australia
[57] Department of Physics, University of Rijeka, Omladinska 14, 51000 Rijeka, Croatia
[58] Department of Computing, Technische Universität Wien, Wieder Hauptst. 8-10, A-1040 Vienna, Austria
[59] South African Astronomical Observatory, P.O. Box 9 Observatory 7925, South Africa
[60] Space Telescope Science Institute, 3700 San Martin Drive, Baltimore, MD 21218, USA
Received 2012 April 21; accepted 2012 July 3; published 2012 August 13

ABSTRACT

High-magnification microlensing events provide an important channel to detect planets. Perturbations near the peak of a high-magnification event can be produced either by a planet or a binary companion. It is known that central perturbations induced by both types of companions can be generally distinguished due to the essentially different magnification pattern around caustics. In this paper, we present a case of central perturbations for which it is difficult to distinguish the planetary and binary interpretations. The peak of a lensing light curve affected by this perturbation appears to be blunt and flat. For a planetary case, this perturbation occurs when the source trajectory passes the negative perturbation region behind the back end of an arrowhead-shaped central caustic. For a binary case, a similar perturbation occurs for a source trajectory passing through the negative perturbation region between two cusps of an astroid-shaped caustic. We demonstrate the degeneracy for two high-magnification events of OGLE-2011-BLG-0526 and OGLE-2011-BLG-0950/MOA-2011-BLG-336. For OGLE-2011-BLG-0526, the χ^2 difference between the planetary and binary model is $\sim$3, implying that the degeneracy is very severe. For OGLE-2011-BLG-0950/MOA-2011-BLG-336, the stellar binary model is formally excluded with $\Delta\chi^2 \sim 105$ and the planetary model is preferred. However, it is difficult to claim a planet discovery because systematic residuals of data from the planetary model are larger than the difference between the planetary and binary models. Considering that two events observed during a single season suffer from such a degeneracy, it is expected that central perturbations experiencing this type of degeneracy is common.

Key words: Galaxy: bulge – gravitational lensing: micro

Online-only material: color figures

1. INTRODUCTION

Microlensing constitutes one of the major methods to detect and characterize extrasolar planets (Mao & Paczyński 1991; Gould 1992). The method is sensitive to planets that are difficult to be detected by using other methods such as cool planets at or beyond the snow line (Bond et al. 2004; Gaudi et al. 2008; Dong et al. 2009; Sumi et al. 2010; Muraki et al. 2011) and planets at large distances (Janczak et al. 2010). It is also sensitive to low-mass planets (Beaulieu et al. 2006; Bennett et al. 2008), making it possible to detect terrestrial planets from ground observations. Due to the weak dependence on the host-star brightness, it also enables us to detect planets around low-mass stars down to M-type dwarfs (Udalski et al. 2005; Miyake et al. 2011; Batista et al. 2011) and even to sub-stellar mass objects. It is the only method that can detect old planetary-mass objects that are not bound to stars (Sumi et al. 2011). In addition, microlensing is the only technique that can detect planets located in external galaxies such as the Magellanic Clouds and the Andromeda galaxy (Chung et al. 2006; Ingrosso et al. 2009). Therefore, microlensing is important for the complete census of the frequency and properties of planets (Gould et al. 2010; Cassan et al. 2012).

Current microlensing planet searches are being conducted based on a specially designed strategy where survey and follow-up observations work in close coordination. There are two main reasons for this strategy. The first reason is that the probability

[61] The OGLE Collaboration.
[62] Author to whom any correspondence should be addressed.
[63] The MOA Collaboration.
[64] The μFun Collaboration.
[65] The MiNDSTEp Consortium.
[66] Royal Society University Research Fellow.
[67] The PLANET Collaboration.
[68] The RoboNet Collaboration.

of a lensing event is very low. For a star located in the Galactic bulge, toward which planetary microlensing searches are being conducted, the chance to detect a lensed star at a specific time is of the order of 10^{-6} (Udalski et al 1994; Alcock et al. 2000; Afonso et al. 2003; Sumi et al 2003). Considering that a planet can be detected for a small fraction of lensing events, it is essential to maximize the detection rate of lensing events to increase the rate of planet detections. Survey observations are designed for this purpose by monitoring a large area of the Galactic bulge field. The second reason for the survey/follow-up strategy is that the duration of a planetary signal is short. The planetary signal is a short-term perturbation to the smooth standard light curve of the primary-induced lensing event. To densely cover planetary perturbations, follow-up observations are designed to focus on events detected by survey observations.

Under the current strategy of microlensing searches, high-magnification events are important targets for follow-up observations. A typical number of events alerted at a certain time by survey experiments are of the order of 10. Considering that each event typically lasts for several dozens of days, it is difficult to follow all alerted events with a restricted number of telescopes. To maximize the planet detection efficiency, priority is given to events for which the planet detection probability is high. Currently, the highest priority is given to high-magnification events. For a lens with a planet, two sets of disconnected caustics exist, where one set is located away from the planet-host star (planetary caustic) while the other set is always located close to the host star (central caustic). The caustics represent the positions on the source plane at which the lensing magnification of a point source becomes infinite. For a high-magnification event, the sensitivity to a planetary companion is very high because the source trajectory always passes close to the perturbation region around the central caustic induced by the planet (Griest & Safizadeh 1998). The efficiency of the strategy focusing on high-magnification events is demonstrated by the fact that 7 out of 13 microlensing planets detected as of the end of 2011 were detected through this channel.

Perturbations near the peak of a high-magnification lensing event (central perturbations) can be produced not only by a planet but also by a binary companion (Han & Hwang 2009; Shin et al. 2012). For a binary lens where the projected separation between the lens components is substantially smaller than the Einstein radius (close binary), a small single set of caustics formed around the barycenter of the binary exists. For a binary where the projected separation is substantially larger than the Einstein radius (wide binary), on the other hand, two sets of caustics each of which is located close to each lens component exist. Then, for a high-magnification event resulting from the source trajectory passing close to the center of mass of a close binary or close to one of the lens components of a wide binary, there can be a short-term perturbation near the peak of the lensing light curve, similar to the central perturbation induced by a planet. It is known that the central perturbation induced by a planet can be generally distinguished from that induced by a binary because the caustic shapes and the resulting magnification patterns around the two types of caustics are different from each other.

In this paper, we present a case of central perturbations for which it is difficult to distinguish between the planetary and binary interpretations. In Section 2, we describe details of the degeneracy. In Section 3, we demonstrate the degeneracy for two microlensing events OGLE-2011-BLG-0526 and OGLE-2011-BLG-0950/MOA-2011-BLG-336 that were detected during the 2011 observation season. In Section 4, we summarize the results and conclude.

2. DEGENERACY

The pattern of central perturbations in a lensing light curve is basically determined by the shape of the central caustic. For both planetary and binary cases, the central caustics form a closed figure that is composed of concave curves that meet at cusps. The general magnification pattern is that a positive perturbation occurs when the source is located in the region outside the caustic extending from cusps while a negative perturbation occurs when the source is located in the region between cusps. Here a "positive" ("negative") perturbation means that the magnification of the perturbed part of the light curve is higher (lower) than the magnification of the corresponding single-lensing event. The origin of the positive and negative perturbations is the reflection of the sum rule for lensing magnification in the region around caustic cusps (Blandford & Narayan 1986; Schneider & Weiss 1992; Zakharov 1995; Petters et al. 2001; Keeton et al. 2003). The central caustics induced by a planet and a binary companion have different shapes and thus the resulting patterns of magnification around the two types of caustics are different from each other. In Figure 1, we present the central caustics and the magnification patterns around them for the representative cases of the planetary and binary lenses, respectively.

The central caustic induced by a planet has a shape of an arrowhead with four cusps. One cusp corresponding to the sharp tip of the arrowhead-shaped caustic is located on the star–planet axis. This cusp is strong in the sense that light curves resulting from source trajectories passing close to the cusp exhibit strong deviations from the single-lens expectation. Two other cusps are located off the star–planet axis corresponding to the blunt ends of the arrowhead-shaped caustic. These two cusps are moderately strong. The fourth cusp, which is located on the star–planet axis between the two off-axis cusps, is weak in the sense that it creates relatively weak deviations. Due to the weakness of the last cusp, an extended region of negative perturbation between the two off-axis cusps exists.

The central caustic induced by a wide or a close binary has an astroid shape with four cusps. Two of the cusps are located on the binary-lens axis and the other two are along a line perpendicular to the axis. The caustic is exactly symmetric with respect to the line connecting the on-line axis cusps and roughly symmetric with respect to the line connecting the off-axis cusps. Due to the symmetry of the caustic, all cusps are of roughly similar strength. Regions of positive perturbations form outside the caustic extending from the cusps and regions of negative perturbations form between the positive-perturbation regions.

Despite the basically different caustic shapes and the resulting magnification patterns, we find a case of central perturbations for which it is difficult to distinguish between the planetary and binary interpretations. This degeneracy is illustrated in Figures 1 and 2. The planetary lensing case for this degeneracy occurs when the source trajectory passes the negative perturbation region behind the back end of the arrowhead-shaped central caustic with an angle between the source trajectory and the star–planet axis (source-trajectory angle) of $\alpha \sim 90^{\circ}$. For a binary case, a similar perturbation occurs when the source trajectory passes through the negative perturbation region between two cusps of an astroid-shaped caustic with a source-trajectory angle of $\sim 45^{\circ}$. For both cases, the morphology of the resulting

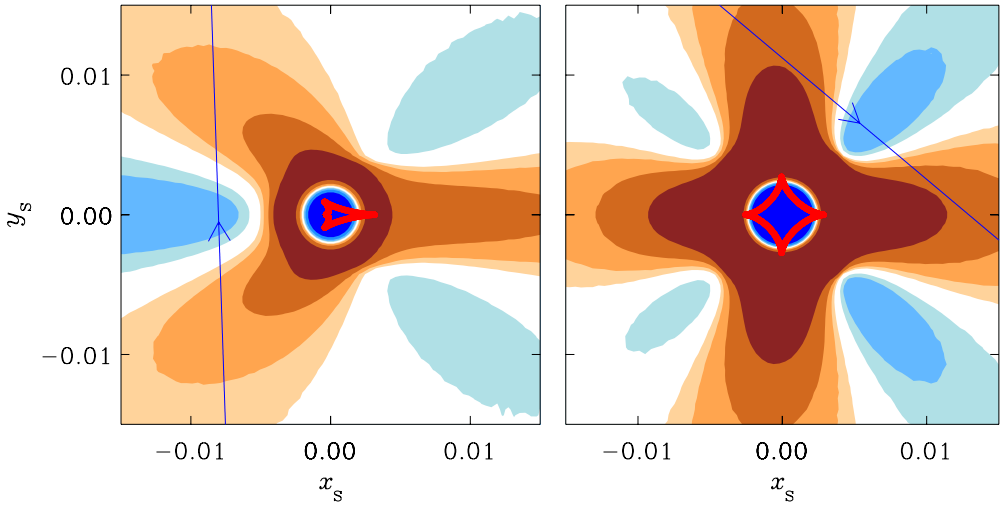

Figure 1. Central caustics induced by a planetary (left panel) and a binary companion (right panel). The regions with brownish and bluish colors represent the areas where the lensing magnification is higher and lower than the corresponding single-lensing magnification, respectively. For each tone, the color changes to darker shades when the fractional difference between the single and binary magnification is >2%, 4%, 8%, and 16%, respectively.

(A color version of this figure is available in the online journal.)

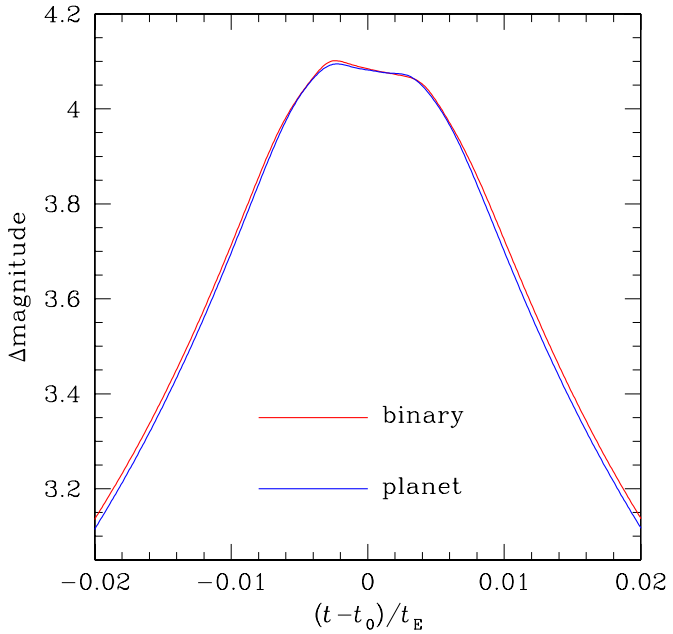

Figure 2. Light curves resulting from the two source trajectories (straight lines with arrows) marked in Figure 1. The notations t_0 and t_E in the label represent the time of the closest lens-source approach and the timescale required for the source to cross the Einstein radius, respectively.

(A color version of this figure is available in the online journal.)

perturbation is that the peak of the light curve appears to be blunt and flat.

3. ACTUAL EVENTS

We search for high-magnification events with similar central perturbations among those detected during the 2011 observation season. From this search, we find that two events of OGLE-2011-BLG-0526 and OGLE-2011-BLG-0950/MOA-2011-BLG-336 exhibit such central perturbations. In this section, we investigate the severity of the degeneracy by conducting detailed modeling of the light curves for these events.

The event OGLE-2011-BLG-0526 occurred on a Galactic bulge star that is positioned at $(\alpha, \delta)_{J2000} = (18^{\rm h}02^{\rm m}45\overset{\rm s}{.}37, -28^\circ01'25\overset{''}{.}8)$, which correspond to the Galactic coordinates $(l, b) = (2\overset{\circ}{.}69, -2\overset{\circ}{.}79)$. The event was detected and alerted to the microlensing community by the Optical Gravitational Lensing Experiment (OGLE) group. High-magnification events are usually realerted after the first alert. Unfortunately, no high-magnification alert was issued for this event and thus the peak was covered by using a fraction of telescopes available for follow-up observations. As a result, the coverage of the peak is not very dense. The telescopes used for the observations of this event are listed in Table 1.

The event OGLE-2011-BLG-0950/MOA-2011-BLG-336 also occurred on a Galactic bulge star located at $(\alpha, \delta)_{J2000} = (17^{\rm h}57^{\rm m}16\overset{\rm s}{.}63, -32^\circ39'57\overset{''}{.}0)$, corresponding to $(l, b) = (358\overset{\circ}{.}07, -4\overset{\circ}{.}05)$. It was independently discovered from the survey experiments conducted by the OGLE and the Microlensing Observation in Astrophysics (MOA) groups. A high-magnification alert was issued for this event four days before the peak. Based on this alert, follow-up observations were conducted by using 13 telescopes located in 8 different countries. As a result, the perturbation was more densely covered than the perturbation of OGLE-2011-BLG-0526. In Table 1, we also list the telescopes used for the observations of this event.

Initial reductions of the data taken from different observatories were processed by using photometry codes developed by the individual groups. For the purpose of improving the data quality, we conducted additional photometry for all follow-up data of OGLE-2011-BLG-0950/MOA-2011-BLG-336 by using codes based on difference imaging photometry. For the use of modeling based on different data sets, it is necessary to rescale error bars of the individual data sets to prevent over or under representation of some data sets. We rescaled the error bars of the data sets so that χ^2 per degree of freedom becomes unity for each data set, where the value of χ^2 is calculated based on the best-fit solution obtained from modeling. We eliminated 3σ outliers from the best-fit solution in the modeling. For some lensing data sets, especially with faint baseline brightness, it is occasionally found that the error estimation near the peak and the baseline is inconsistent. For both events analyzed in this work, however, the photometric precision is good and thus the dependence of the lensing parameters on the normalization procedure is weak.

Table 1
Telescopes

Event	Telescopes
OGLE-2011-BLG-0526	OGLE 1.3 m Warsaw telescope at Las Campanas Observatory in Chile
	MiNDSTEp 1.54 m Danish telescope in Chile
	PLANET 0.6 m at Perth Observatory in Australia
	PLANET 1.0 m at SAAO in South Africa
	RoboNet 2.0 m Liverpool telescope (LT) in La Palma, Spain
OGLE-2011-BLG-0950/	OGLE 1.3 m Warsaw telescope at Las Campanas Observatory in Chile
MOA-2011-BLG-336	MOA 1.8 m at Mt. John Observatory in New Zealand
	μFUN 1.3 m SMARTS telescope at CTIO in Chile
	μFUN 0.4 m at Auckland Observatory in New Zealand
	μFUN 0.4 m at Farm Cove Observatory (FCO) in New Zealand
	μFUN 0.4 m at Kumeu Observatory in New Zealand
	μFUN 0.6 m at Observatorio do Pico Dos Dias (OPD) in Brazil
	μFUN 1.0 m at Wise Observatory in Israel
	MiNDSTEp 1.54 m Danish telescope in Chile
	PLANET 1.0 m at SAAO in South Africa
	RoboNet 2.0 m Faulkes Telescope North (FTN) in Hawaii
	RoboNet 2.0 m Faulkes Telescope South (FTS) in Australia
	RoboNet 2.0 m Liverpool telescope (LT) in La Palma, Spain

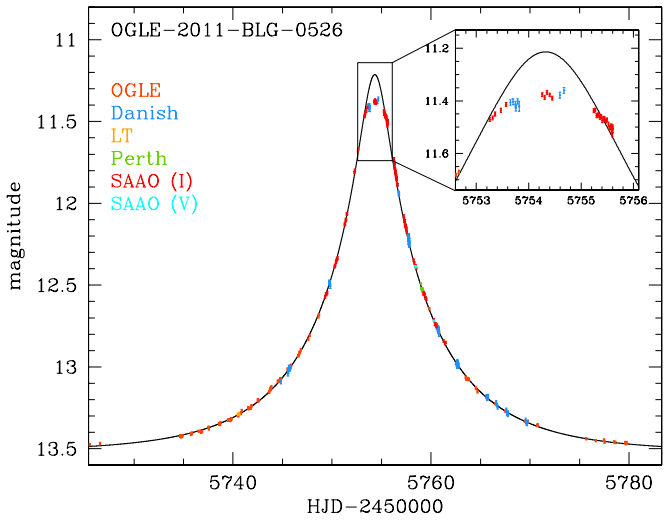

Figure 3. Light curve of OGLE-2011-BLG-0526. Also drawn is the best-fit single-lensing light curve that is obtained with data except those around the perturbation. Colors of data points are chosen to match those of the labels of observatories where the data were taken. The inset shows the enlarged view of the peak region.

(A color version of this figure is available in the online journal.)

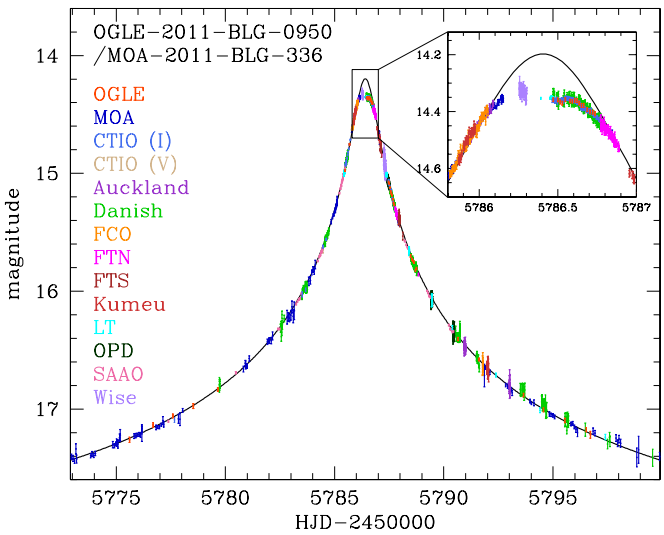

Figure 4. Light curve of OGLE-2011-BLG-0950/MOA-2011-BLG-336. Notations are the same as those in Figure 3.

(A color version of this figure is available in the online journal.)

In Figures 3 and 4, we present the light curves of the two events. The best-fit single-lensing light curves are also drawn. For both events, the light curves are well represented by those of standard single-lensing events except for the short-lasting perturbations near the peak. The common morphology of the perturbations is that the peak appears to be flat and blunt.

To investigate the nature of the perturbations, we conducted binary-lens modeling of the light curves. In the modeling of each light curve, we searched for the solution of the binary-lensing parameters that best describe the observed light curve by minimizing χ^2 in the parameter space. For OGLE-2011-BLG-0526, the timescale of the event is not long ($t_{\rm E} \sim 12$ days) and thus we modeled the light curve using seven basic binary-lens parameters. The first three of these parameters characterize the geometry of the lens-source approach and they include the Einstein timescale, $t_{\rm E}$, the time of the closest lens-source approach, t_0, and the lens-source separation at that moment, u_0, in units of the Einstein radius. Another three parameters characterize the binary lens. These parameters include the mass ratio between the lens components, q, the projected separation in units of the Einstein radius, s, and the angle between the source trajectory and the binary axis, α. The last parameter of the normalized source radius $\rho_\star$ describes the deviation of the light curve affected by the finite-source effect and it represents the angular source radius $\theta_\star$ in units of the angular Einstein radius $\theta_{\rm E}$, i.e., $\rho_\star = \theta_\star/\theta_{\rm E}$. For OGLE-2011-BLG-0950/MOA-2011-BLG-336, the duration of the event ($t_{\rm E} \sim 65$ days) is relatively long. For such a case, the motion of the source with respect to the lens may deviate from a rectilinear one due to the change of the observer's position caused by the orbital motion of the Earth around the Sun and this deviation can cause a long-term deviation in the light curve (Gould 1992). Consideration

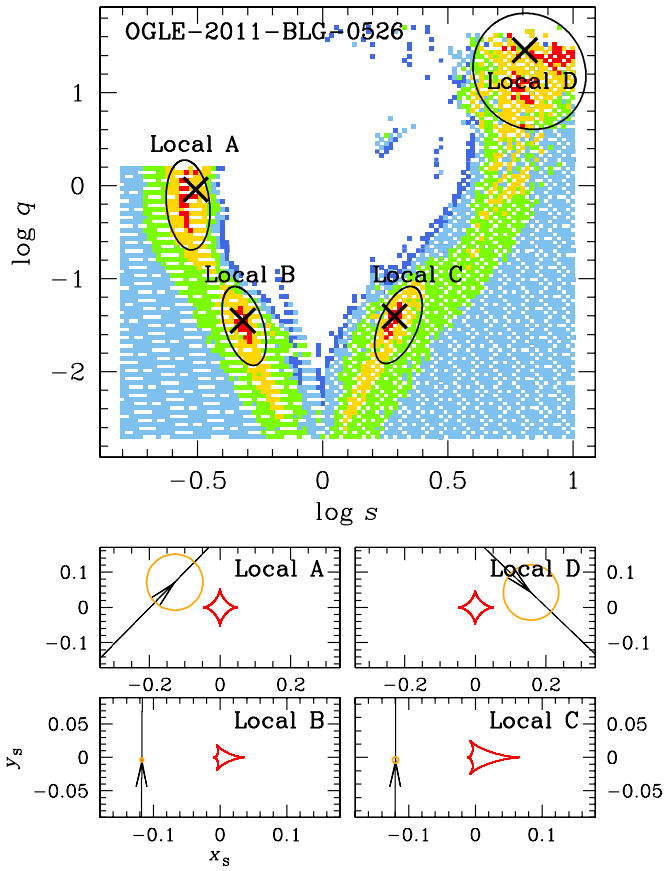

Figure 5. Map of $\Delta\chi^2$ in the parameter space of the projected binary separation (s) and the mass ratio (q) for OGLE-2011-BLG-0526. The regions marked in red, yellow, green, sky blue, and blue correspond to those with $\Delta\chi^2 < 6^2$, 12^2, 18^2, 24^2, and 30^2, respectively. The cross marks represent the locations of the local minima. The lower panels show the source trajectories (straight lines with arrows) with respect to the caustics for the individual local solutions. The orange circle on each source trajectory represents the relative scale of the source star.

(A color version of this figure is available in the online journal.)

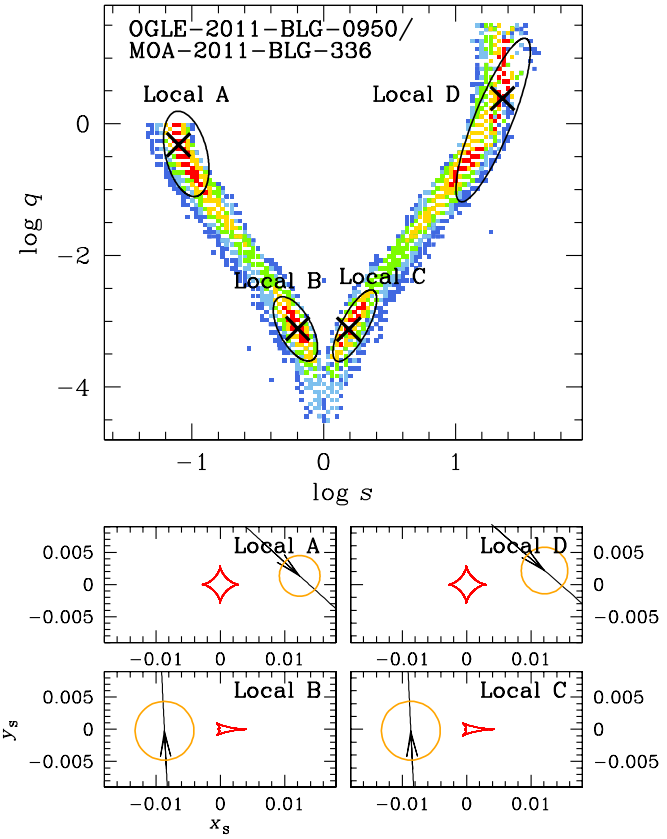

Figure 6. Map of $\Delta\chi^2$ in the s–q parameter space for OGLE-2011-BLG-0950/MOA-2011-BLG-336. The regions marked in red, yellow, green, sky blue, and blue correspond to those with $\Delta\chi^2 < 13^2$, 26^2, 39^2, 52^2, and 65^2, respectively. Notations are the same as in Figure 5.

(A color version of this figure is available in the online journal.)

of this "parallax effect" requires us to include two additional parameters $\pi_{\mathrm{E},N}$ and $\pi_{\mathrm{E},E}$, which represent the two components of the lens parallax $\boldsymbol{\pi}_{\mathrm{E}}$ projected on the sky in the north and east equatorial coordinates, respectively. The direction of the parallax vector corresponds to the relative lens-source motion in the frame of the Earth at a specific time of the event. Its size corresponds to the ratio of Earth's orbit to the physical Einstein radius, $r_{\mathrm{E}} = D_L\theta_{\mathrm{E}}$, projected on the observer plane, i.e., $\pi_{\mathrm{E}} = (\mathrm{AU}/r_{\mathrm{E}})[(D_{\mathrm{S}} - D_{\mathrm{L}})/D_{\mathrm{S}}]$.

Knowing that central perturbations can be produced either by a planet or by a binary companion, we conduct a thorough search for solutions in the s–q parameter space encompassing both planet and binary regimes to investigate the possible existence of local minima. In Figures 5 and 6, we present the resulting maps of $\Delta\chi^2$ in the s–q parameter space for the individual events. From the maps, it is found that four distinct local minima for both events exist. Among them, two minima are located in the region with $s > 1$ and the other two are located in the region with $s < 1$. For each close/wide binary pair, one local minimum is located in the regime of a binary mass ratio ($q \sim 1$) and the other minimum is located in the regime of a planet mass ratio ($q \ll 1$). We designate the individual minima by "A" ($s < 1$ with binary q), "B" ($s < 1$ with planetary q), "C" ($s > 1$ with planetary q), and "D" ($s > 1$ with binary q).

In Table 2, we present the lensing parameters of the individual local minima that are obtained by further refining the local solutions in the corresponding parameter space. The exact locations of the local minima are marked by "X" on the $\Delta\chi^2$ maps in Figures 5 and 6. For each local solution, we also present the caustic and the source trajectory. We note that the size of the caustic for the binary with $s < 1$ is scaled by the Einstein radius corresponding to the total mass of the lens, while the caustic size for the binary with $s > 1$ is scaled by the Einstein radius corresponding to the mass of the lens component that the source approaches.

The findings from the comparison of the local solutions and the corresponding lens-system geometries are summarized as below.

1. For both events, χ^2 differences from the best-fit single-lensing models are very big. We find that $\Delta\chi^2 = 1085$ for OGLE-2011-BLG-0526 and $\Delta\chi^2 = 5644$ for OGLE-2011-BLG-0950/MOA-2011-BLG-336, implying that the perturbations of both events are clearly detected.
2. Despite the clear signature of the perturbation, we find that the degeneracy of the four local solutions is severe. To better show the subtle differences between the local solutions, we present the residuals of the data from the individual local solutions in Figures 7 and 8 for OGLE-2011-BLG-0526 and OGLE-2011-BLG-0950/MOA-2011-BLG-336, respectively. We also present the enlargement of the

Table 2
Best-fit Parameters

Parameter	OGLE-2011-BLG-0526				OGLE-2011-BLG-0950/MOA-2011/BLG-336			
	A	B	C	D	A	B	C	D
χ^2/dof	423.6/413	420.0/413	422.2/413	422.9/413	3073.5/3096	2968.6/3096	2969.0/3096	3076.9/3096
t_0	5754.24 ± 0.01	5754.35 ± 0.01	5754.35 ± 0.01	5754.24 ± 0.01	5786.40 ± 0.01	5786.40 ± 0.01	5786.40 ± 0.01	5786.40 ± 0.01
u_0	0.141 ± 0.001	0.117 ± 0.002	0.117 ± 0.002	0.140 ± 0.020	$(9.3 \pm 0.1)10^{-3}$	$(8.6 \pm 0.1)10^{-3}$	$(8.7 \pm 0.1)10^{-3}$	$(9.0 \pm 0.3)10^{-3}$
$t_{\rm E}$ (days)	11.63 ± 0.08	12.15 ± 0.09	12.37 ± 0.10	11.60 ± 1.91	61.39 ± 0.67	65.21 ± 0.85	65.27 ± 0.76	62.41 ± 1.90
s	0.311 ± 0.003	0.48 ± 0.01	1.94 ± 0.02	6.43 ± 0.05	0.075 ± 0.001	0.70 ± 0.01	1.43 ± 0.01	22.7 ± 0.3
q	0.91 ± 0.04	$(3.5 \pm 0.2)10^{-2}$	$(3.9 \pm 0.2)10^{-2}$	28.5 ± 10.6	0.83 ± 0.09	$(5.8 \pm 0.2)10^{-4}$	$(6.0 \pm 0.2)10^{-4}$	2.36 ± 0.21
α	-0.795 ± 0.010	4.718 ± 0.004	4.718 ± 0.004	0.765 ± 0.007	0.739 ± 0.005	4.664 ± 0.002	4.664 ± 0.002	0.722 ± 0.002
$\rho_\star$ (10^{-3})	80 ± 2	...	...	79 ± 7	3.2 ± 0.3	4.6 ± 0.1	4.6 ± 0.1	3.4 ± 0.3
$\pi_{{\rm E},N}$	...	...	...	...	0.22 ± 0.15	-0.10 ± 0.17	-0.29 ± 0.14	0.12 ± 0.09
$\pi_{{\rm E},E}$	...	...	...	...	-0.04 ± 0.03	0.02 ± 0.03	0.03 ± 0.02	-0.03 ± 0.02

Notes. The mass ratio with $q > 1.0$ represents that the source trajectory approaches close to the lower-mass component of the binary lens.

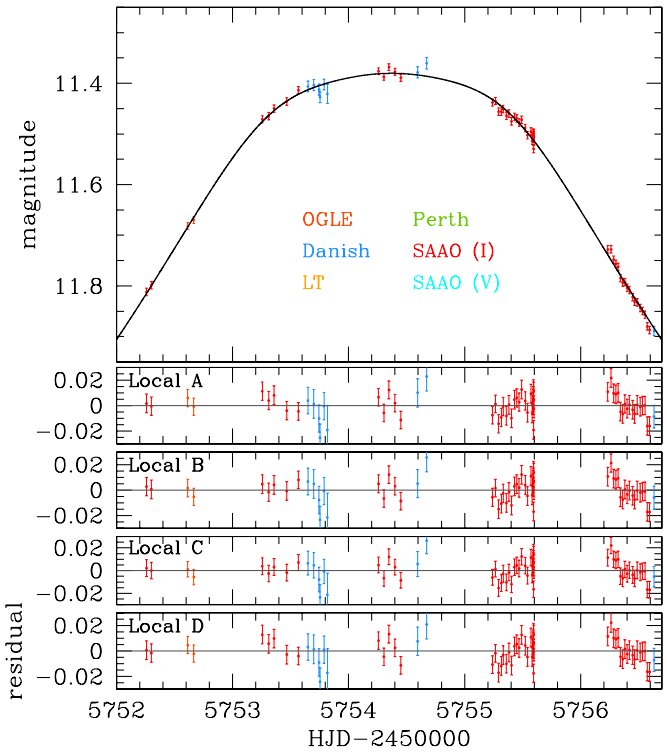

Figure 7. Light curve of OGLE-2011-BLG-0526 near the peak region and the residuals from four local solutions. The model light curve drawn over the data is based on one of the local solutions (local "B"). Colors of data points are chosen to match those of the labels of observatories where the data were taken.

(A color version of this figure is available in the online journal.)

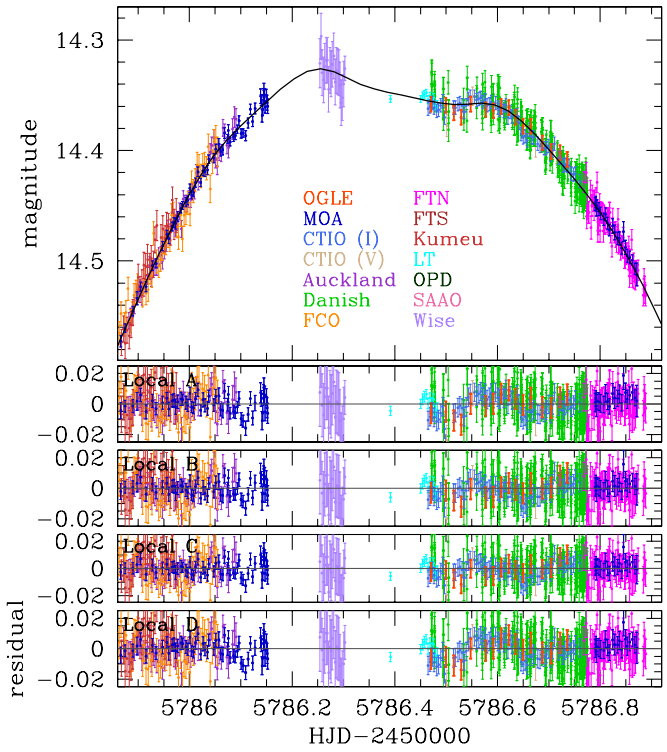

Figure 8. Light curve of OGLE-2011-BLG-0950/MOA-2011-BLG-336 near the peak region and the residuals from four local solutions. The model light curve drawn over the data is based on one of the local solutions (local "C"). Notations are the same as those in Figure 7.

(A color version of this figure is available in the online journal.)

perturbed parts of the light curve in the upper panel of each figure. For the case of OGLE-2011-BLG-0526, the χ^2 difference between the planetary and binary models is $\sim$3, implying that the degeneracy is very severe. For the case of OGLE-2011-BLG-0950/MOA-2011-BLG-336, the planetary solution is favored over the binary solution with $\Delta\chi^2 \sim 105$ and thus the stellar binary model is formally excluded. However, from the visual inspection of the residuals, it is found that systematic residuals of the data from the planetary model are larger than the difference between the planetary and binary models. In addition, the CTIO, Danish, and OGLE data of overlapping coverage appear to be different from each other by an amount at least as large as the difference between the planetary and stellar binary models. Therefore, it is difficult to claim a planet discovery based on $< 1\%$ variations in the light curve.

3. For a pair of solutions with similar mass ratios, the solutions with $s > 1$ and $s < 1$ result in a similar caustic shape. The degeneracy between these solutions, often referred to as $s \leftrightarrow s^{-1}$ degeneracy, is known to be caused by the symmetry of the lens-mapping equation between close and wide binaries (Dominik 1999; Albrow et al. 1999; Afonso et al. 2000; An 2005; Chung et al. 2005).

The degeneracy between the pairs of solutions with planetary and binary mass ratios corresponds to the degeneracy mentioned in Section 2. Note that despite the large difference in caustic shape, the resulting perturbations appear to be very alike. The planet/binary degeneracy introduced in this work was not known before. This is mostly because the caustics induced by a planet and a binary companion have very different shapes and thus it is widely believed that perturbations induced by the two types of companions can be easily distinguished. Considering that two events of a single season suffer from this degeneracy, it is expected that central perturbations suffering from this is common.

4. CONCLUSION

We introduced a new type of degeneracy in the planet/binary interpretation of central perturbations in microlensing light curves. The planetary lensing case for this degeneracy occurs when the source trajectory passes the negative perturbation region behind the back end of the arrowhead-shaped central caustic with a source-trajectory angle of $\sim$90°. For a binary case, a similar perturbation occurs when the source trajectory passes through the negative perturbation region between two cusps of an astroid-shaped caustic with a source-trajectory angle of $\sim$45°. For both cases, the morphology of the resulting perturbation is that the peak of the light curve appears to be blunt and flat. From an investigation of events detected during the 2011 microlensing observation season, we found two events, OGLE-2011-BLG-0526 and OGLE-2011-BLG-0950/MOA-2011-BLG-336, which exhibit such perturbations. From detailed modeling of the light curves, we demonstrated the severity of the degeneracy. Considering that two events during a single season suffer from the degeneracy, we conclude that central perturbations experiencing the degeneracy should be common.

Work by C.H. was supported by the Creative Research Initiative Program (2009-0081561) of the National Research Foundation of Korea. The OGLE project has received funding from the European Research Council under the European Community's Seventh Framework Programme (FP7/2007-2013)/ERC

grant agreement No. 246678. The MOA experiment was supported by grants JSPS22403003 and JSPS23340064. T.S. was supported by the grant JSPS23340044. Y. Muraki acknowledges support from JSPS grants JSPS23540339 and JSPS19340058. The MiNDSTEp monitoring campaign is powered by ARTEMiS (Automated Terrestrial Exoplanet Microlensing Search; Dominik et al. 2008). M.H. acknowledges support by the German Research Foundation (DFG). D.R. (boursier FRIA), O.W. (FNRS research fellow), and J. Surdej acknowledge support from the Communauté française de Belgique Actions de recherche concertées, Académie universitaire Wallonie-Europe. K.A., D.M.B., M.D., K.H., M.H., C.L., C.S., R.A.S., and Y.T. are thankful to Qatar National Research Fund (QNRF), member of Qatar Foundation, for support by grant NPRP 09-476-1-078. C.S. received funding from the European Union Seventh Framework Programme (FPT/2007-2013) under grant agreement 268421. This work is based in part on data collected by MiNDSTEp with the Danish 1.54 m telescope at the ESO La Silla Observatory. The Danish 1.54 m telescope is operated based on a grant from the Danish Natural Science Foundation (FNU). A. Gould and B. S. Gaudi acknowledge support from NSF AST-1103471. B. S. Gaudi, A. Gould, and R. W. Pogge acknowledge support from NASA grant NNG04GL51G. Work by J. C. Yee is supported by a National Science Foundation Graduate Research Fellowship under Grant No. 2009068160. S. Dong's research was performed under contract with the California Institute of Technology (Caltech) funded by NASA through the Sagan Fellowship Program. Research by T.C.H. was carried out under the KRCF Young Scientist Research Fellowship Program. T.C.H. and C.U.L. acknowledge the support of Korea Astronomy and Space Science Institute (KASI) grant 2012-1-410-02. Dr. David Warren provided financial support for Mt. Canopus Observatory.

REFERENCES

Afonso, C., Alard, C., Albert, J. N., et al. 2000, ApJ, 532, 340
Afonso, C., Albert, J. N., Alard, C., et al. 2003, A&A, 404, 145
Albrow, M., Beaulieu, J.-P., Caldwell, J. A. R., et al. 1999, ApJ, 522, 1022
Alcock, C., Allsman, R. A., Alves, D. R., et al. 2000, ApJ, 541, 734
An, J. H. 2005, MNRAS, 356, 1409
Batista, V., Gould, A., Dieters, S., et al. 2011, A&A, 529, 102
Beaulieu, J.-P., Bennett, D. P., Fouqué, P., et al. 2006, Nature, 439, 437
Bennett, D. P., Bond, I. A., Udalski, A., et al. 2008, ApJ, 684, 663
Blandford, R., & Narayan, R. 1986, ApJ, 310, 568
Bond, I. A., Udalski, A., Jaroszyński, M., et al. 2004, ApJ, 606, L155
Cassan, A., Kubas, D., Beaulieu, J.-P., et al. 2012, Nature, 481, 167
Chung, S.-J., Han, C., Park, B.-G., et al. 2005, ApJ, 630, 535
Chung, S.-J., Kim, D., Darnley, M. J., et al. 2006, ApJ, 650, 432
Dominik, M. 1999, A&A, 349, 108
Dominik, M., Horne, K., Allan, A., et al. 2008, Astron. Nachr., 329, 248
Dong, S., Bond, I. A., Gould, A., et al. 2009, ApJ, 698, 1826
Gaudi, B. S., Bennett, D. P., Udalski, A., et al. 2008, Science, 319, 927
Gould, A. 1992, ApJ, 392, 442
Gould, A., Dong, S., Gaudi, B. S., et al. 2010, ApJ, 720, 1073
Griest, K., & Safizadeh, N. 1998, ApJ, 500, 37
Han, C., & Hwang, K.-H. 2009, ApJ, 707, 1264
Ingrosso, G., Calchi Novati, S., De Paolis, F., et al. 2009, MNRAS, 399, 219
Janczak, J., Fukui, A., Dong, S., et al. 2010, ApJ, 711, 731
Keeton, C. R., Gaudi, B. S., & Petters, A. O. 2003, ApJ, 598, 138
Mao, S., & Paczyński, B. 1991, ApJ, 374, L37
Miyake, N., Sumi, T., Dong, S., et al. 2011, ApJ, 728, 120
Muraki, Y., Han, C., Bennett, D. P., et al. 2011, ApJ, 741, 22
Petters, A. O., Levine, H., & Wambsganss, J. 2001, Singularity Theory and Gravitational Lensing (Boston: Birkhäuser)
Schneider, P., & Weiss, A. 1992, A&A, 260, 1
Shin, I.-G., Choi, J.-Y., Park, S.-Y., et al. 2012, ApJ, 746, 127
Sumi, T., Abe, F., Bond, I. A., et al. 2003, ApJ, 591, 204
Sumi, T., Bennett, D. P., Bond, I. A., et al. 2010, ApJ, 710, 1641
Sumi, T., Kamiya, K., Bennett, D. P., et al. 2011, Nature, 473, 349
Udalski, A., Jaroszyński, M., Paczyński, B., et al. 2005, ApJ, 628, L109
Udalski, A., Szymański, M., Stanek, K. Z., et al. 1994, Acta Astron., 44, 165
Zakharov, A. F. 1995, A&A, 293, 1